



STRUCTURAL DESIGN AND STRENGTH ANALYSIS OF PARTS OF THE HYDRAULIC ARM INTENDED TO BE MOUNTED ON LIGHT TRUCK CHASSIS

Miroslav BLATNICKÝ, Ján DIŽO*

* University of Žilina, Faculty of Mechanical Engineering

Univerzitná 8215/1, 010 26 Žilina, Slovak Republic, e-mail: miroslav.blatnický@fstroj.uniza.sk,
jan.dizo@fstroj.uniza.sk

Abstract

The paper deals with the structural design and strength calculations using analytical and numerical method for a hydraulic arm to be mounted on the light truck chassis. The whole arm is made up of three parts of the steel structure, namely a cranking arm, a lifting arm, and a slewing column. We approached to strength calculations of these three parts of the hydraulic arm individually, using two methods to verify the safety of the designed structure. Loading of the arm will be induced by a burden of the total maximum weight = 300 kg.

Key words: hydraulic arm, strength calculation, dimensioning, FEM analysis, stability

INTRODUCTION

Mankind's many years of development to the state that we are witnessing nowadays originated in the distant past, when man had to struggle for survival in the original living conditions. The process of repeating successful activities, which have brought improvements of living conditions, gave rise also to the development of brain activity from simple logic operations, through memorising, to analysing the knowledge. This process resulted in the products of man that were gradually improved, which lead to construction of mechanisms and machines. This process of developing technical systems that free man of repetitive physical labour is called mechanisation.

There is no need to discuss too much on the importance of mechanisation in handling loads. If we want the handling equipment to operate properly, mechanisation must be an essential part thereof. The level of mechanisation is strongly influenced by several factors. For example, if mechanisation is not accompanied with a guarantee of a high degree of safety, then effective mechanisation cannot even be implemented. Technical equipment including such parts of mechanisms that allow a perfect and reliable transfer of force effects is a crucial prerequisite for successful mechanisation [4]. An important task for engineers is to analyse the in-use and newly designed work processes in order to find an optimal way to carry out the given operation. Generally, the best work process is considered the one that minimises the cost required to provide the performance, which can again be achieved through mechanisation. Mechanisation represents an important means of

raising productivity, quality and competitiveness of manufacture/production. Successful introduction and implementation of mechanisation requires the knowledge and understanding of physical dependences of the operations carried out. Operations are carried out through the transfer of mechanical, electrical, pneumatic or hydraulic energy. The aim is that individual work tasks be as short and as simple as possible, and make them easy to learn. At the same, the work tasks should require minimal exercise of manpower. Mechanisation significantly frees man from heavy physical labour, for example in a dangerous or harmful environment or conditions. A mechanisation means of the above-mentioned kind is the proposed and designed hydraulic arm (Figure 1), which significantly facilitates the handling process due to its high operability. Applying the condition of minimum production costs we can achieve the most efficient performance/cost ratio [2].

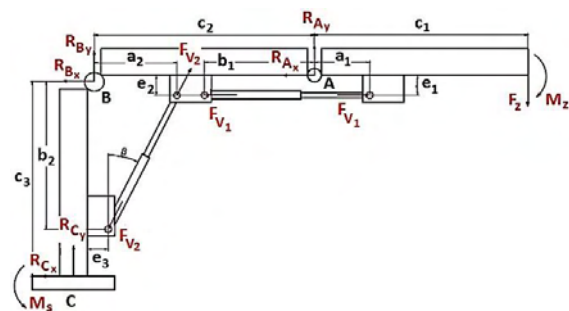


Fig. 1. Preliminary draft design of the arm showing the geometry and loading force effects

1. FUNCTIONAL CALCULATION OF FORCES AND MOMENTS IN THE ARM

One of the partial objectives of this paper is to utilise analytical calculation to arrive at preliminary force effects on the arm that will be loaded with a maximum load weight $m = 300$ kg. Figure 1 shows the structural diagram of the proposed and designed arm mechanism, defining the length dimensions at the position of its maximum radius (sweep reach).

The proposed lengths of the individual parts that result from the hydraulic motor construction, as will be set forth in this paper, are as follows: $c_1 = 1150$ mm, $c_2 = 1150$ mm, $c_3 = 887$ mm, $e_1 = e_2 = e_3 = 75$ mm, $a_1 = a_2 = 210$ mm, $b_1 = b_2 = 774$ mm [2]. Functioning of the arm is ensured by two hydraulic cylinders. We will later calculate the hydraulic cylinder's proper dimensions and the resulting force ratios. The entire steel structure of the mechanism consists of three parts. The column (dimension c_3 in Figure 1), i.e. one of the three parts, does not move at work in either of the directions. However, the column structural design allows rotational movement about its axis, also securing its movement from one side of the car to another using a movement mechanism (mover). Arms c_1 and c_2 will be able to perform, thanks to the hydraulic cylinders and rotary bonds, movement in two directions (in fact, this is rotation in plane represented by this "sheet of paper"), thereby ensuring handling of loads in the entire hydraulic arm overhang (radius) space. Cost-effective production of this mechanism can be achieved using normalised (standard) profiles. Our calculations of the force effects on the arm are based on the three basic equilibrium equations (1):

$$\begin{aligned} \sum F_{ix} &= 0, \\ \sum F_{iy} &= 0, \\ \sum M_i &= 0. \end{aligned} \quad (1)$$

These equations are applicable to all three parts of the arm. The following applies to the first part of the arm c_1 (Figure 1) from equations (1):

$$\begin{aligned} F_{HM1} - R_{Ax} &= 0, \\ R_{Ax} - F_z &= 0, \\ -F_z \cdot c_1 + F_{HM1} \cdot e_1 &= 0. \end{aligned} \quad (2)$$

To the second part of the arm c_2 (Figure 1), the following applies from equations (1):

$$\begin{aligned} R_{Ax} - R_{Bx} + F_{HM2} \cdot \sin \beta - F_{HM1} &= 0, \\ -R_{Ay} - R_{By} + F_{HM2} \cdot \cos \beta &= 0, \\ F_{HM2} \cdot a_2 \cdot \cos \beta + F_{HM2} \cdot e_2 \cdot \sin \beta - \\ -R_{Ax} \cdot c_2 - F_{HM1} \cdot e_1 &= 0. \end{aligned} \quad (3)$$

The angle β in the position shown (Figure 1), which is the most effective position of the load to induce maximum forces in hydraulic motors, is calculated using equation (4):

$$\beta = \operatorname{tg}^{-1} \cdot \frac{a_2 - e_3}{b_2 - e_2}. \quad (4)$$

The following applies to the third part of the arm c_3 (Figure 1) from equations (1), (2) and (3):

$$\begin{aligned} R_{Bx} - F_{HM2} \cdot \sin \beta + R_{Cx} &= 0, \\ R_{By} - F_{HM2} \cdot \cos \beta + R_{Cy} &= 0, \\ R_{Bx} \cdot c_3 + F_{HM2} \cdot \cos \beta \cdot e_3 - \\ -F_{HM2} \cdot \sin \beta (c_3 - b_2) - M_S &= 0. \end{aligned} \quad (5)$$

Then, the calculated values of forces and moments are as follows: $R_{Ay} = 2943$ N, $R_{Ax} = 45126$ N, $F_{V1} = 45126$ N, $F_z = 2943$ N, $F_{V2} = 30710$ N, $R_{Bx} = 5823$ N, $R_{By} = 27210$ N, $R_{Cy} = 2943$ N and $M_S = 6827$ Nm.

One can see that internal force effects produce the same moment as a load suspended at the end of the mechanism. We can therefore assume that the internal force effects calculation is correct. Therefore, we can select a suitable hydraulic motor. We found from the calculated values that the maximum force to be provided by the linear hydraulic motor is $F_{V1} = 45126$ N.

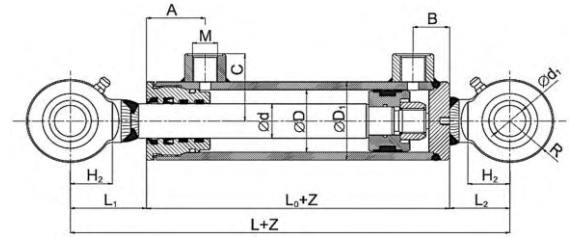


Fig. 2. Linear hydraulic motor

Comparing this figure with the parameters declared by the manufacturer indicates that EH series linear hydraulic motors (cylinder diameter $D = 63$ mm, the sum of hydraulic motor meshes distances from the cylinder $L = 224$ mm, hydraulic motor stroke $Z = 380$ mm, hydraulic motor mesh diameter $d_1 = 25$ mm, outer hydraulic motor cylinder diameter $D_1 = 73$ mm, hydraulic motor piston rod diameter $d = 32$ mm) are sufficient and compliant (Figure 2).

The provisionally chosen arm geometry is appropriate when using hydraulic motors of the above geometry. Therefore, the calculations are accurate enough and the arm geometry needs no further optimisation. Correctly determined force effects in the proposed mechanism are a necessary precondition for the safe operation of this device. The next step in addressing this issue is analytical calculation of cross-sectional dimensions of individual parts of the arm, using conventional methods of material elasticity and strength, as well as numerical methods using a computer.

2. ANALYTICAL DIMENSIONAL CALCULATION OF A PART OF THE ARM

In this section we will carry out a model analytical dimensional calculation of the first part of the arm. We will determine and plot stress patterns in the first part of the arm, based on which we will determine the necessary arm dimensions. In order to ensure safety of the structure, we chose safety level $k = 1.5$ (-). We chose the material STN 11 423 to manufacture the arm steel structure because of the material suitable mechanical properties, guaranteed weldability and relatively low cost. We choose normalised (standardised) quadrangular seamless steel tubes formed by heat. Provisionally we choose the profile TR4 HR 90x70x5-11 423.0 STN 42 5720 [1] (Figure 3). Thus, we admit permissible combined stress of the steel structure $\sigma_{reddov} = 120$ MPa [1] within the above-mentioned safety level. We will carry out analytical calculation using conventional methods of material elasticity and strength to determine stress values in the first part of the arm. We consider the body as a beam with precise geometry and load (Figure 4). The load size was addressed in the previous chapter.

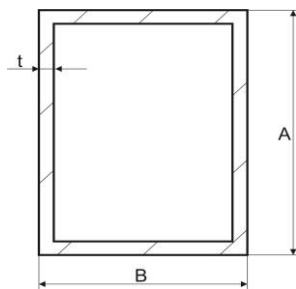


Fig. 3. The profile chosen for the hydraulic arm construction

Calculation of the bending moment as the dominant load is carried out using the imaginary cut method.

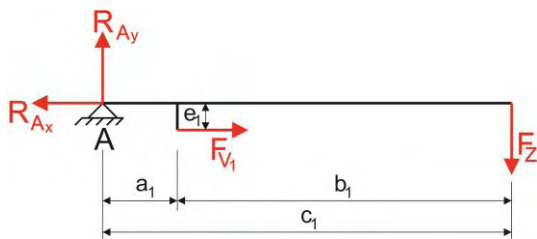


Fig. 4. Geometry and release of the first part of the arm

We cut the beam as many times as it is divided by external load, internal load and geometry – in this case we cut two times (Figure 5).

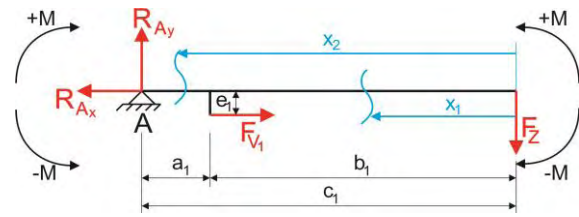


Fig. 5. Marking the sites of imaginary cuts on the beam

Designation of the force F_{V1} in Figures 4 and 5 is equivalent with the force F_{V1} in the calculations from equations (1). The following applies to the bending moment M_o in the first field in Figure 5 (6):

$$x_1 \in \langle 0, b_1 \rangle, \tag{6}$$

$$M_{o(x_1)} = -F_z \cdot x_1.$$

Solving this equation results in the bending moment values in boundary conditions 0 and b_1 (7):

$$M_{o(x_1=0)} = -2943 \cdot 0 = 0 \text{ Nmm},$$

$$M_{o(x_1=b_1)} = -2943 \cdot 940 = -2766420 \text{ Nmm} = -2766.420 \text{ Nm}. \tag{7}$$

The following applies to the axial force T in the first field in Figure 5:

$$x_1 \in \langle 0, b_1 \rangle, \tag{8}$$

$$T = 0 \text{ N}.$$

The following applies to the bending moment M_o in the second field in Figure 5 (9):

$$x_2 \in \langle b_1, b_1 + a_1 \rangle, \tag{9}$$

$$M_{o(x_2)} = -F_z \cdot x_2 + F_{V1} \cdot e_1.$$

Solving this equation results in the bending moment values in boundary conditions b_1 and $b_1 + a_1$ (10):

$$M_{o(x_2=b_1)} = -2943 \cdot 940 + 45126 \cdot 75 = 618030 \text{ Nmm} = 618.03 \text{ Nm},$$

$$M_{o(x_2=b_1+a_1)} = -2943 \cdot (940 + 210) + 45126 \cdot 75 = 0 \text{ Nmm}. \tag{10}$$

The following applies to the axial force T in the second field in Figure 5:

$$T = F_{V1} = 45126 \text{ N}. \tag{11}$$

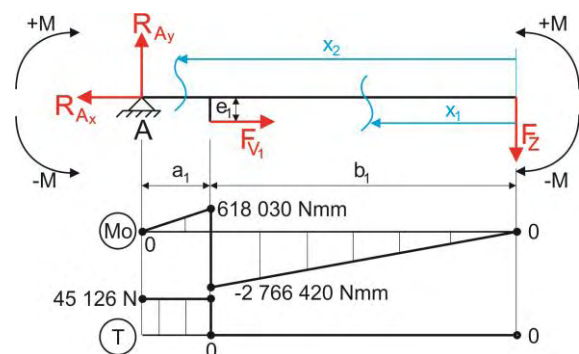


Fig. 6. Progressions of moments and axial forces in the beam

Figure 6 shows the progressions of moments and displacing forces in the beam under consideration 6. Dimensions of the chosen pipe profile form Figure 3 are as follows: $A = 90$ mm, $B = 70$ mm, $t = 5$ mm, $a = 80$ mm, $b = 60$ mm. Then, the following applies to the value of section modulus of bending W_o (12):

$$W_o = \frac{BA^3 - ba^3}{6 \cdot A} = \frac{70 \cdot 90^3 - 60 \cdot 80^3}{6 \cdot 90} = 37611.11 \text{ mm}^3, \quad (12)$$

and the stress σ_o will be (13):

$$\sigma_o = \frac{M_{o \max}}{W_o} = \frac{2766420}{37611.11} = 73.55 \text{ MPa}. \quad (13)$$

A disadvantage of calculating the maximum stress size using the analytical method resides in the definition of critical cross section, because analytically we can relate the calculation to one particular surface area or cross section. This cross section is rather difficult to define and can be executed as an estimate only. Figure 7 shows the determined critical cross section. The stress state at the site of the greatest bending moment is shown in Figure 7. As can be seen, lower filaments will be pressure (compression) stressed and upper filaments in part 1 will be tension stressed.

The greatest bending moment, and thus the greatest stress is assumed at the site shown in Figure 7. However, the stress size will still increase significantly. This is caused by the axial force effect in the beam second field, as well as by additional bending moment caused by the force from the hydraulic motor F_{V1} acting on the hydraulic motor holder at the distance e_1 from the marginal filament (the site where the largest bending moment acts from the force F_z). Figure 8 shows acting of the stress state arising from this force due to the holder.

The size of the cross-sectional area S_1 of the first part of the arm results from the dimensions A , a , B , b shown in Figure 3. Then, the cross-sectional area will be (14):

$$S_1 = A \cdot B - (A - 2t) \cdot (B - 2t) = 90 \cdot 80 - (90 - 2 \cdot 5) \cdot (70 - 2 \cdot 5) = 1500 \text{ mm}^2 = 0.0015 \text{ m}^2. \quad (14)$$

The stress size from the axial force T (eq. 11) will be:

$$\sigma_o = \frac{F}{S} = \frac{T}{S_1} = \frac{45126}{1500} = 30.084 \text{ MPa}. \quad (15)$$

The resulting stress from the bending moment and the axial force will be as follows (16):

$$\sigma_v = \sigma_o + \sigma_a = 73.55 + 30.084 = 103.634 \text{ MPa}. \quad (16)$$

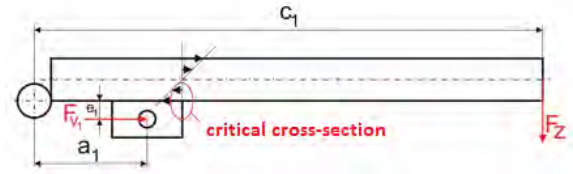


Fig. 7. Position of the considered critical cross section

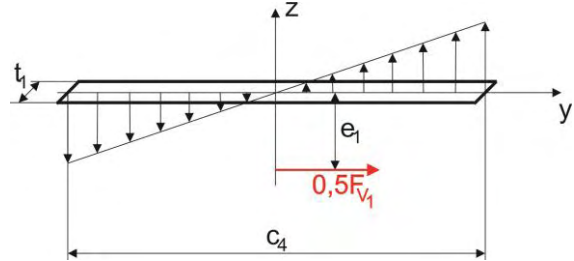


Fig. 8. Stress state arising from the hydraulic motor force F_{V1} in the plane of the body 1 contact with the hydraulic motor holder

Figure 8 shows half the force from the hydraulic motor, because there are two holders with apertures through which the pin passes, carrying the hydraulic motor mesh. The holder has a rectangular cross section, and it is necessary to calculate the required cross-sectional characteristics to determine additional stress values. Thus, the critical cross section is at the site where the seamless rectangular pipe overlaps with the holder for mounting the hydraulic motor. In addition to the bending moment that results in the stress state shown in Figure 8, it is necessary to consider also the shear effect of the force F_{V1} , therefore the resulting stress in the plane of contact of these two bodies will increase again. Let us choose the holder dimensions for example from the condition of material 11 423 impression at the site of contact of the pin and the holder aperture. Permissible stress for impression within the safety level $k = 1.5$ (-) is considered as $p_{dov} = 63$ MPa. Then, the following applies (17):

$$p = \frac{F}{S} = \frac{F_{V1}}{2 \cdot d_c \cdot t_1} \leq p_{dov}. \quad (17)$$

The pin diameter depends on the hydraulic motor construction design, and is thus identical to the hydraulic motor mesh aperture for the pin, i.e. $d_c = 25$ mm:

$$t_1 \geq \frac{45126}{2 \cdot 25 \cdot 63} = 14.325 \text{ mm}. \quad (18)$$

We choose $t_1 = 15$ mm. Based on the shear stress in the plane of the weld seam of part 1 and the holder in Figure 8 we choose the holder length $c_4 = 200$ mm. Thus, the section modulus in bending W_{Od} of the holder in the plane of contact of the holder and the first part of the arm, considering the sense of the acting force F_{V1} , is as follows (19):

$$W_{Od} = \frac{1}{6} \cdot c_4^2 \cdot t_1 = \frac{1}{6} \cdot 200^2 \cdot 15 = 100000 \text{ mm}^3. \quad (19)$$

The bending moment M_{Od} on one holder from the hydraulic motor force F_{V1} will be as follows (20):

$$M_{Od} = \frac{F_{V1} \cdot e_1}{2} = \frac{45126 \cdot 75}{2} = 1692225 \text{ Nmm} = 1692.225 \text{ Nm}, \quad (20)$$

and the stress size σ_{Od} will be (21):

$$\sigma_{Od} = \frac{M_{Od}}{W_{Od}} = \frac{1692255}{1000000} = 16.93 \text{ MPa}. \quad (21)$$

Then, the resulting normal stress σ_N will be as follows (22):

$$\sigma_N = \sqrt{\sigma_V^2 + \sigma_{Od}^2} = \sqrt{103.634^2 + 16.93^2} = 105 \text{ MPa}. \quad (22)$$

The shear stresses $\tau_{S\parallel}$ caused by the force F_{V1} and $\tau_{S\perp}$ by the force F_{V2} in the plane of contact of the hydraulic motor holder and part 1 of the hydraulic arm will be (23a, 23b):

$$\tau_{S\parallel} = \frac{F}{S} = \frac{F_{V1}}{2 \cdot c_4 \cdot t_1} = \frac{45126}{2 \cdot 200 \cdot 15} = 7.521 \text{ MPa}, \quad (23a)$$

$$\tau_{S\perp} = \frac{F}{S} = \frac{F_{V2}}{2 \cdot c_4 \cdot t_1} = \frac{30710}{2 \cdot 200 \cdot 15} = 5.118 \text{ MPa}. \quad (23b)$$

The reduced stress σ_{red} in the plane of contact of the hydraulic motor holder and part 1 of the hydraulic arm will be (24):

$$\sigma_{red} = \sqrt{\sigma_N^2 + 3 \cdot \tau_S^2} = \sqrt{105^2 + 3 \cdot 7.521^2} = 106 \text{ MPa}. \quad (24)$$

The observed value of reduced maximum stress in the critical cross section may not fully correspond to the actual stress in a real structure. One of the reasons is neglecting own weight of the first part of the arm, which is considered in the numerical calculation.

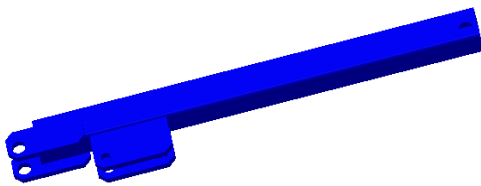


Fig. 9. 3D model of the first part of the arm

There is also the effect of stress raiser that represents a step change in the arm part 1 section with the hydraulic motor holder, which was not considered in the calculation. It is necessary to multiply the observed value by the stress raiser coefficient α . Despite the fact that the coefficient α depends only on the component geometry and its stresses, its determination in real structures is rather difficult. This coefficient is most commonly determined by experimental methods [3 and 5] (photoelasticity, miniature tensometric strings, etc.), or by applying numerical methods (finite element method, geometric element method, etc.) [11]. Analytically, it is possible to determine the size of α only for elementary cases of planar and rotation symmetrical (axisymmetric) problems of elasticity

and strength at a limited number of variable factors. Therefore, it will be helpful to carry out numerical calculation of this structure where we can expect an increased stress value directly in the critical section – in particular at the stress raiser site. After analytical calculations it is possible to make an accurate 3D model of the first part of the structure using the CAD CATIA system (Figure 9). All dimensions of the first part of the arm fully correspond to the entered and calculated values of lengths and cross sections.

3. NUMERICAL DIMENSIONAL CALCULATION OF PARTS OF THE ARM

Nowadays there are many computer tools allowing investigation of strength and dynamic analysis [12 and 13] of individual bodies or complex structure [6, 7, 8 and 9]. Finite Element Method the most commonly used numerical technique based on the continuum mechanics [10 and 11] allowing mainly the investigation and determination of the stresses and strains in materials and structures subjected to forces, torques etc.

If the local extreme of stress (in the critical cross section) is below the permissible value of 120 MPa, then the first part of the arm is correctly dimensioned within the chosen safety level, and its optimisation is not necessary. To check the dimensions accuracy we will carry out numerical calculation using a FEM software and compare the results to find simulated values of stress.

Numerical simulation (Figure 10) has proven the assumption of the analytical solution of the site with the greatest stress in part 1 of the hydraulic arm. The value 117 MPa indicated by the software is about 9 % higher than the result of the analytical solution. Here, the result has manifested of the absence of a stress raiser coefficient whose exact value is difficult to determine, as well as the load increment due to the arm weight. The structure was modelled using shell 181 elements, with the mesh density 5 mm and a free form meshing algorithm. Boundary conditions fully respected the actual manner of mounting and loading the structure. In this way we managed to use analytical and numerical calculations to solve the first part of the small hydraulic lifting arm with versatile use. The next step in addressing this issue will be analytical and numerical solving of the remaining two parts of this mechanism. After designing all dimensions it will be possible to create an accurate 3D model of the entire structure in CAD software.

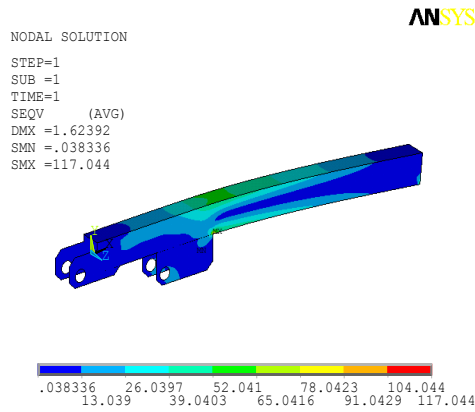


Fig. 10. Effective stress distribution in the first part of the hydraulic arm due to the load in the most effective position

Correctly determined sections and thus compliance with the design stresses (Figure 11) in this mechanism are essential prerequisites for the safe operation of this device. Thus constructed model will then be imported into MBS software where we will observe the structure dynamic properties during operation.

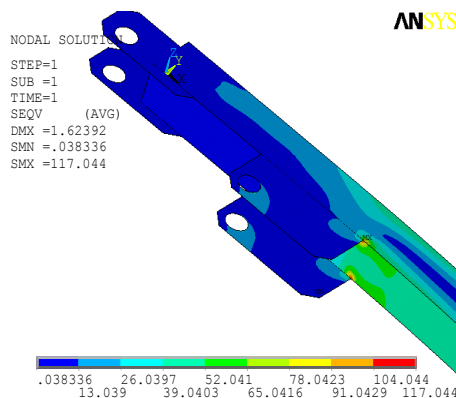


Fig. 11. Detail of the critical section with simulated effective stress

3.1 Central part of the arm

Like in the previous case, we chose safety level $k = 1.5$ (-) to ensure the structure safety. We chose the STN 11 423 material to manufacture the arm steel structure because of the material suitable mechanical properties, guaranteed weldability and relatively low cost.

We choose normalised (standardised) quadrangular seamless steel tubes formed by heat. Provisionally we choose the profile TR4 HR 120x100x6-11 423.0 STN 42 5720. Thus, we admit permissible combined stress of the steel structure $\sigma_{reddov} = 120$ MPa within the above-mentioned safety level. We will carry out analytical calculation using conventional methods of material elasticity and strength to determine stress values in the central part of the arm (Figure 12).

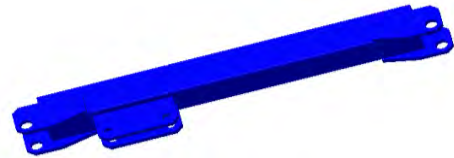


Fig. 12. 3D model of the central part of the arm

We consider the body as a beam with precise geometry and load, the size of which was addressed in the previous step.

Calculation of the bending moment as the dominant load is carried out using the imaginary cut method. We cut the beam as many times as it is divided by external load, internal load and geometry – in this case we cut three times (Figure 13). Since there is some similarity with the first part of the arm, analytical calculation will only be partial, without intermediate results obtained.

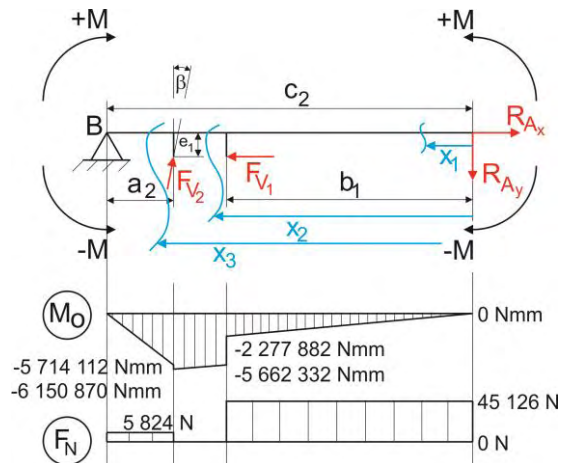


Fig. 13. Progressions of moments and normal forces in the beam

Thus, in addition to bending stress state, pressure stress state also acts at the critical cross section due to the normal force $F_N = 5824$ N. Then, the following applies to the total stress (25):

$$\sigma_c = \frac{M_{o_{max}}}{W_o} + \frac{F_N}{S}. \quad (25)$$

Solving equation (25) we obtain the value of the total stress $\sigma_c = 73.8$ MPa. The force from the hydraulic motor F_{V1} further stresses the critical cross section through the holder by shear stress parallel to the structure length, and the force from the hydraulic motor F_{V2} stresses the critical cross section through the holder by shear stress as well, but this shear stress is perpendicular to the structure length. We determine the value of this resulting shear stress using equation (26):

$$\tau_s = \sqrt{\tau_{s\parallel}^2 + \tau_{s\perp}^2}. \quad (26)$$

Values of the components $\tau_{s\parallel}$ and $\tau_{s\perp}$ are given by equations 23a and 23b, respectively. Then, the resulting shear stress in the critical cross section will be $\tau_s = 9.1$ MPa. Reduced stress on the critical cross section is calculated according to HMH hypothesis

(27):

$$\sigma_{RED} = \sqrt{\sigma_c^2 + 3 \cdot \tau_s^2} \tag{27}$$

Using the analytical method of calculation, the reduced stress value in the weld reaches $\sigma_{RED} = 75.5$ MPa. Analytical calculations showed that the chosen geometry is compliant and able to withstand the load. However, the resulting stress value will increase even more due to neglecting the structure own weight in analytical calculation. Therefore, it is appropriate to verify the accuracy of analytical calculation by FEM analysis of the structure.

We modelled the addressed structure using the Adina FEM software. We entered the structure's material properties into the software program (elasticity modulus $E = 2.1e11$ Pa, density $\rho = 7850$ kg.m⁻³, Poisson's ratio $\mu = 0.3$, that is all parameters were the same as in the first part of the arm). For meshing we used four-node tetrahedral elements with 4-mm mesh density. After running the solver we can display in a post processor the results for equivalent von Mises stress (Figure 14).

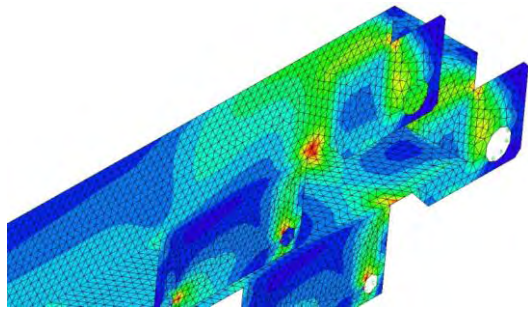


Fig. 14. Distribution of equivalent von Mises stress in the structure

The values as well the site of the maximum stress found by ADINA software are virtually identical to the analytical calculation. Using ADINA software, stress values in the critical cross section can be set within the range of 80–86 MPa compared to 75.5 MPa from the analytical calculation. Figure 15 shows detail of the critical site with equivalent stress distribution.

The numerical calculation carried out using ADINA software has confirmed that the position of the critical cross section was again estimated correctly. The calculated stress size is again smaller than the permissible values for the material from which the structure is made. Therefore, the second part of the arm is designed correctly.

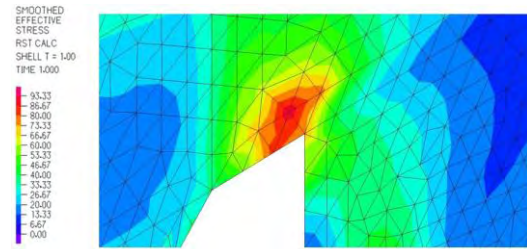


Fig. 15. Detail of equivalent stress distribution in the critical cross section

3.2. Hydraulic arm column

At this point we determine the section modulus, based on which we choose a normalised (standardised) type of blank. Then we check the blank whether it is able to withstand the specified load. Again we find the progressions of the bending moment and axial forces, and we plot the progressions afterwards. In this case, we have to cut the beam in two fields (Figure 16).

Calculation of the section modulus W_o is based on the condition for calculation of the bending stress (28):

$$\sigma_o = \frac{M_{o\max}}{W_o} \leq \sigma_{Do} \tag{28}$$

The maximum value of the bending moment M_{Omax} is shown in Figure 16. We consider permissible bending stress 75 MPa. Then, the bending section modulus according to (28) must be as follows:

$$W_o \geq \frac{6768853.242}{75} = 90251.37 \text{ mm}^3 \tag{29}$$

When choosing the profile we have to meet the requirement of having the section modulus of the chosen profile higher than, or at most equal to, the value we have calculated in the previous step.

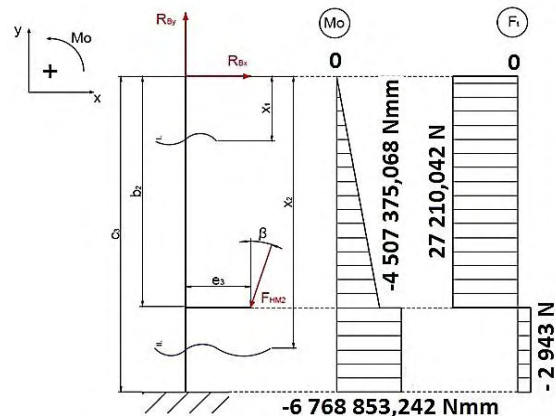


Fig. 16. Progressions of moments and axial forces in the column

The chosen section dimensions: TR 4 HR 120 x 100 x 8 – 5 000 – 11 423.0 – STN 42 5720. At the same time, corresponding with Figure 3, the following applies: $A = 120$ mm, $B = 100$ mm, $t = 8$ mm, $a = 104$ mm, $b = 84$ mm. Then, the chosen profile section modulus will be according to

equation (12):

$$W_o \geq \frac{100 \cdot 120^3 - 84 \cdot 104^3}{6 \cdot 120} = 108765.867 \text{ mm}^3. \quad (30)$$

The chosen profile type must be verified by analytical calculation in order check whether the generated stresses do not exceed the permissible limit. Check calculation must also take into consideration the effect of tensile or compressive force, and the additional bending moment as well. These effects are caused by the force from the hydraulic motor F_{V2} acting on the hydraulic motor holder (Figure 17). We estimate the critical cross section position to be at the site depicted in Figure 17.

While respecting equations (4–24), using analytical calculation we obtain 89.05 MPa as the value of reduced stress.

Again, this value is lower than the admissible 120 MPa. However, since the calculation neglected the column own weight, it will be appropriate to carry out numerical calculation of this structure.

When entering the same material properties, and respecting the actual mounting and loading of the structure, i.e. respecting the boundary conditions, we can execute this calculation. The model was actually mounted (Figure 18) and actually loaded (Figure 19).

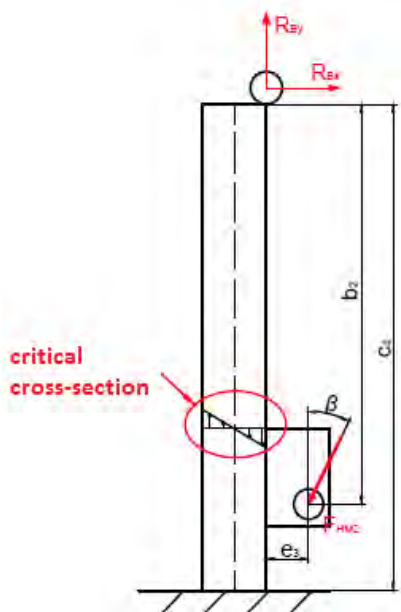


Fig. 17. Position of the considered critical cross section

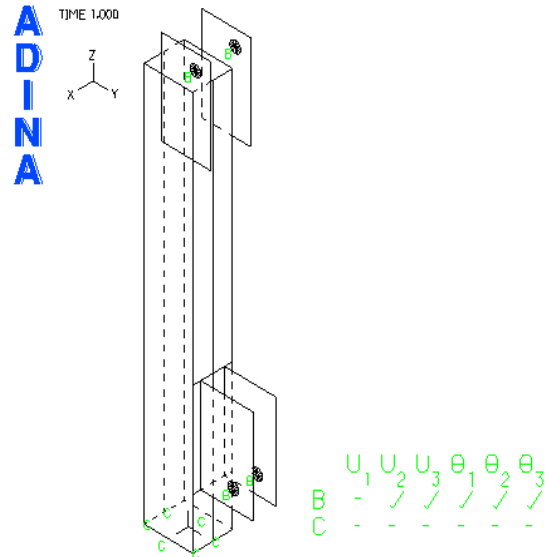


Fig. 18. Removing degrees of freedom of the column

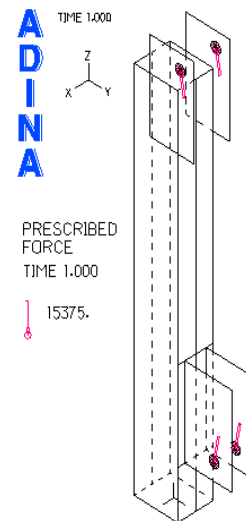


Fig. 19. Load on the arm column

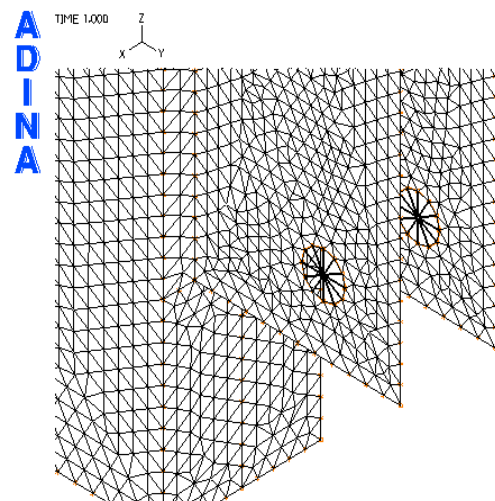


Fig. 20. Detail of the arm column mesh

To mesh the model (Figure 20) we used linear tetrahedral elements with the element size of 4 mm. After running the solver we can display in a post processor the results for equivalent von Mises stress (Figure 21). It follows from the simulation that the chosen profile is designed correctly, since the stress acting in the structure is lower than the permissible one. Thus, we can conclude that the chosen profile is able to withstand the load.

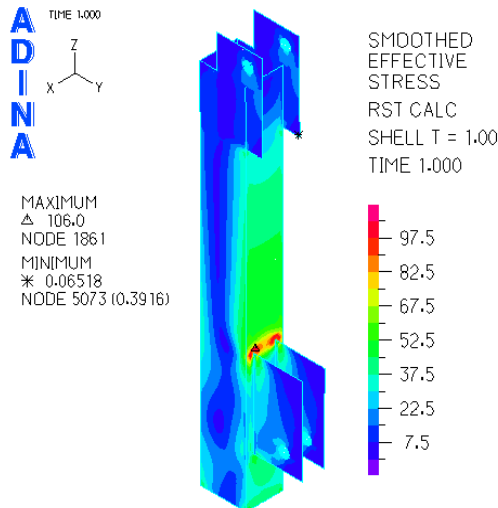


Fig. 21. Equivalent stress distribution in the column

Since all parts of the arm were designed and checked using analytical and numerical calculations, it is possible to create an accurate 3D model of the structure (Figure 22). When creating the model, we have to follow from the already entered and calculated values.

Each part of the hydraulic arm (Figures 9, 12 and 22) was individually modelled using CATIA V5 software. We have also modelled the components to join individual parts of the mechanism (connecting pins, welds, hydraulic motors).

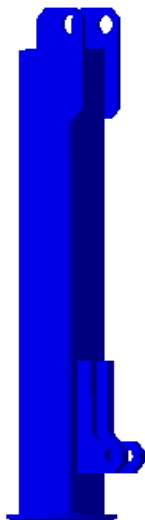


Fig. 22. 3D model of the hydraulic arm column

4. SUMMARY

The purpose of this paper was to create conceptual designs, and utilise analytical and numerical calculations to address a small hydraulic lifting arm (Figure 23) with multifunction and versatile use.

Since the numerical calculation has verified the accuracy of the analytical solution, it can be concluded that the purpose has been met. The next step in addressing this issue will be entering the model into MBS software, where dynamic responses of the device behaviour will be monitored during its use. It will be necessary to address the stability of vehicle on which this device will be mounted when working on a flat surface. We will also need to determine the maximum lateral inclination angle of the vehicle in order to comply with the condition of stability with a certain safety level.



Fig. 23. Designed hydraulic arm

Last but not least, we will have to solve the arm mounting to the platform, ensuring its required motion parameters, as well as to propose and design the drive, control and regulation for the hydraulic motors used. Subsequently, we will attempt to manufacture a prototype that will be tested according to the applicable standards for steel structures.

Acknowledgement

This contribution is the result of the project implementation: “Modern methods of teaching the control and diagnostic systems of engine vehicles”, ITMS code 26110230107, supported by the Operation Programme Education.

REFERENCES

- [1] Balaja J, Bronček J, Antala J, Sekerešová D. Mechanical Engineering Tables. (In Slovak). Selection Standards. Slovak Office of Standards, Metrology and Testing, 2014.
- [2] Blatnický M, Dižo J. Analysis of the hydraulic arm for use on light goods vehicle. In: Production management and engineering sciences. Leiden,

- London: CRC Press/Balkema; Taylor & Francis Group, 2011: 351-354.
- [3] Chernyak A, Gerlici J, Nozhenko O, Domin R, Kravchenko K, Lack T. The experimental research of the dynamic loading of the railway track. In: Experimental and computational method in engineering, 3rd International conference for young scientists. Jun 1-3, 2016, J. E. Purkyně University, Ústí nad Labem, Czech Republic, CD-ROM, 8 pages.
- [4] Galliková J, Poprocký R. Maintenance according to the technical state with use of the enterprise asset management systems. In: Zeszyty naukowe Instytutu Pojazdów: mechanika, ekologia, bezpieczeństwo, mechatronika 2015; 103:67:75
- [5] Gerlici J, Lack T, Harušinec J. Loading collectives for experimental research on the test stand RAILBCOT. In: Dynamics of rigid and deformable bodies 2015, 13th International scientific conference, J. E. Purkyně University, Ústí nad Labem, Czech Republic, October 7-9, 2015, CD-ROM.
- [6] Lack T, Gerlici J. Tangential stresses for non-elliptical contact patches computed by means of a modified FASTSIM method. In: Civil-Comp Proceedings, 2016; online.
- [7] Lack T, Gerlici J. The FASTSIM method modification in speed up the calculation of tangential contact stresses between wheel and rail. In Manufacturing Technology – journal for science, research and production 2013; 13(4): 486-492.
- [8] Lack T., Gerlici J.: Wheel/rail tangential contact stress evaluation by means of the modified strip method. In Komunikacie 2104; 16(3A): 33-39.
- [9] Lack T, Gerlici J. A modified strip method to speed up the tangential stress between wheel and rail calculation. In: Applied Mechanics and Materials 2014; 486: 359-370.
- [10] Maňurová M, Suchánek A. Determination of stiffness of triple spring built in a bogie of a rail vehicle. In: Manufacturing Technology 2016; 16(2): 390-396.
- [11] Pacana J, Kozik B, Budzik G. Strength analysis of gears in dual-path gearing by means of FEM. In: Diagnostyka 2015; 16(1): 41-46.
- [12] Sapietová A, Gajdoš L, Dekýš V, Sapieta M. Analysis of the influence of input function contact Parameters of the impact force Process in the MSC.ADAMS. In: Advanced in Intelligent Systems and Computing 2016; 393: 243-253.
- [13] Šťastniak P. Freight long wagon dynamic analysis in S-curve by means of computer simulation. In: Manufacturing Technology 2015; 15(5): 930-935.



Ing. Miroslav BLATNICKÝ, PhD. received B.Sc., M.Sc. and PhD. degrees in Mechanical Engineering from University of Žilina, respectively. He is currently teaching at the Faculty of Mechanical Engineering, University of Žilina. His area of research is focused on functional and strength calculations and FEM analyses.



Ing. Ján DIŽO, PhD. received B.Sc., M.Sc. and PhD. degrees in Mechanical Engineering from University of Žilina, respectively. He is currently teaching at the Faculty of Mechanical Engineering, University of Žilina. Mr. Dižo's research interests focus on creation of MBS models and dynamic analysis of transport and handling machines.

Received 2016-07-07

Accepted 2016-10-21

Available online 2016-11-21